

Formation mechanisms of recrystallization textures in aluminum sheets based on theories of oriented nucleation and oriented growth

Wei-min MAO, Ping YANG

Department of Materials, State Key Laboratory for Advanced Metals and Materials,
University of Science and Technology Beijing, Beijing 100083, China

Received 13 June 2013; accepted 8 October 2013

Abstract: The recrystallization textures in 95% rolled aluminum sheets with different purities and initial textures were investigated. The effects of recovery levels and the dragging effects induced by impurities on the effective driving force and corresponding behaviors of oriented nucleation and oriented growth during annealing were analyzed. The oriented nucleation is a common behavior in the initial stage of primary recrystallization if the effective driving force in deformed matrix is not too high to reduce the necessity of nucleation period. Oriented growth might appear if the temperature is not too high and the grains, of which the misorientation to matrix is about $40^\circ\langle 111 \rangle$, have enough time and space to expand growth advantages, while certain reduction of effective driving force is also necessary. The recrystallization textures could be changed by controlling initial textures and effective driving forces which can be regulated by recovery levels and dragging effects.

Key words: aluminum; recrystallization; texture; recovery; stored energy; boundary migration

1 Introduction

It is known that grain boundary mobility in aluminum is misorientation dependent, and the velocity of boundary migration could reach the maximal value if the misorientation between two neighboring grains is characterized by a rotation around $\langle 111 \rangle$ axis about 40° , i.e. $40^\circ\langle 111 \rangle$ rotation. The phenomena were confirmed by IBE et al [1] who observed statistically the grain growth behaviors of several hundreds deformed aluminum single crystals during annealing. The systematical investigation offered an important basis of oriented growth (OG), as a mechanism for formation of recrystallization textures. The rapid moving characteristics of $40^\circ\langle 111 \rangle$ rotation were reconfirmed by different aluminum bicrystal [2] and polycrystal [3,4] investigations. The detailed atomistic mechanism of the rapid boundary migration could be interpreted to be close to the $\Sigma 7$ CSL (coincidence site lattice with reciprocal density 7) relationship [5] and the corresponding substructure of the boundaries [6,7]. The OG mechanism predicts that different mobilities of boundaries could lead to formation of special recrystallization textures, of which the orientation relation to deformation textures is about

$40^\circ\langle 111 \rangle$ rotation.

It is known as well, that some recrystallized grains have stronger nucleation advantage and nucleate more frequently during annealing. These nuclei should form somewhere in transition bands [8] by means of strong recovery and polygonization processes of certain substructure in deformed matrix. The substructure with cube orientation indicates strong recovery ability and forms high-angle boundaries easily when it reaches a critical size for growth [9]. The cube substructure has been observed most frequently to turn to cube nuclei, which ensures the formation of strong cube recrystallization texture. The nucleation behavior of cube grains was firstly observed by RIDHA and HUTCHINSON [10] in copper, and is also very common in aluminum alloys [11]. It is obvious that the formation of recrystallization texture is determined here by nucleation process, which is called oriented nucleation (ON), as another mechanism for formation of recrystallization textures.

There has been a long dispute between OG and ON. It is, sometimes, rather confused and hard to identify which one of the two mechanisms is more effective on the formation of recrystallization texture in aluminum. However, the ambiguity might be clarified a little bit

more if the evolution of driving force for recrystallization and its influence on formation of recrystallization texture are considered.

2 Experimental

Three kinds of aluminum samples (H, C and F) with different initial textures before cold rolling were taken from industry hot bands or ingots, in order to observe the influence of initial grain orientations on the behaviors of oriented nucleation during annealing after cold rolling. Sample H1 with 7.6 mm in thickness had high purity hot band containing initial cube texture. Sample H2 including H2-1 and H2-2 was the same hot band. However, its cold rolling sample was cut in such a way that the rolling direction (RD) was 45° away from the RD of hot band, namely, the RD was 45° rotated around the normal direction (ND), so that the initial texture became rotated cube texture $\{100\}\langle 011\rangle$. Commercially pure sample C1 with 6.0 mm in thickness was cut from a forged ingot containing initial $\{112\}\langle 111\rangle$ texture [12]. An aluminum ingot containing Ti and B as elements for grain refinement was forged in two mutually perpendicular directions, so that an initial Goss texture for cold rolling of sample F1 with 6.9 mm in thickness was obtained. The Goss texture became initial inverse Goss texture $\{110\}\langle 110\rangle$ of sample F2 as the RD and TD (transverse direction) of following cold rolling were exchanged. All the aluminum samples were 95% cold rolled, and their compositions, initial textures as well as the parameters for following recrystallization annealing in salt bath are indicated in Tables 1 and 2. The rolled

Table 1 Chemical composition of experimental Al alloys

Sample	Composition, w/%
H1, H2-1, H2-2	Fe: 0.0004, Si: 0.0008, Cu: 0.0003, Al: >99.998
C1	Fe: 0.032, Si: 0.032, Cu: <0.001, Al: >99.9
F1, F2	Fe: 0.0027, Si: 0.0045, Cu: 0.0003, B: 0.0009, Ti: 0.01, Al: 99.98

Table 2 Experimental Al alloys, initial texture and parameters of recrystallization annealing

Sample	Main initial texture before cold rolling	Recrystallization annealing after 95% cold rolling
H1	$\{100\}\langle 001\rangle$	(240 °C, 600 s)+ (300 °C, 10000 s)
H2-1	$\{100\}\langle 011\rangle$	(240 °C, 600 s)+ (300 °C, 10000 s)
H2-2	$\{100\}\langle 011\rangle$	300 °C, 316 s
C1	$\{112\}\langle 111\rangle$	500 °C, 900 s
F1	$\{110\}\langle 001\rangle$, $\{110\}\langle 221\rangle$	(240 °C, 600 s)+ (300 °C, 10000 s)
F2	$\{110\}\langle 110\rangle$, $\{110\}\langle 114\rangle$	(240 °C, 600 s)+ (300 °C, 10000 s)

sample F1 was also annealed directly at 300 °C for 2 s and 10 s without 240 °C pretreatment, in order to observe rapid grain growth process. The microstructures during annealing were observed under optical microscope. $\{111\}$, $\{200\}$, $\{220\}$ and $\{113\}$ incomplete pole figures were determined based on the X-ray diffraction and the necessary orientation distribution functions (ODFs) were calculated.

3 Results and discussion

3.1 Formation of recrystallization texture dominated by ON

Figures 1(a) and (b) give the initial textures of high purity aluminum samples before cold rolling. The initial cube $\{100\}\langle 001\rangle$ and rotated cube $\{100\}\langle 011\rangle$ are clearly to see in samples H1 and H2, respectively. The initial textures resulted in strong S $\{123\}\langle 634\rangle$ and Cu type $\{112\}\langle 111\rangle$ texture respectively after 95% cold rolling (Fig. 1(c)), which indicates the close connection between initial texture and rolling texture in Al [12,13].

The cold-rolled samples H1 and H2-1 were firstly pretreated at 240 °C for 600 s to conduct a strong recovery while the stored energy and driving force for recrystallization were reduced drastically. The samples were then annealed at 300 °C for 10000 s, after which the primary recrystallization was completed. Cube recrystallization texture formed in both samples, while it was much stronger in sample H1. Comparing Figs. 1(a) and (b) with Figs. 2(a) and (b), it looks that the more the cube texture before cold rolling was, the stronger the cube texture after recrystallization became. Cube orientation is generally not a stable one during rolling deformation. However, some cube substructure could survive the rolling deformation [10,14,15]. It is also possible during rolling that some grains shift their orientations in a path, in which certain cell blocks might stagnate as they pass by near cube orientation [8,15]. The survived or stagnated cube substructure indicates stronger nucleation advantage [9], which could nucleate more frequently during annealing [16]. Therefore, the growth of cube grains will determine the formation of cube texture. Its density depends on how much cube substructure has survived the rolling deformation, which is surely initial texture dependent. It is obvious that the formation mechanism of recrystallization texture (Figs. 2(a) and (b)) was dominated by ON.

On the other hand, OG process could also help to form such a strong cube texture in Fig. 2(a), since the misorientation between cube orientation and four variants of rolling S texture in sample H1 (Fig. 1(c)) is just about 40° $\langle 111\rangle$, which could lead to rapid growth of

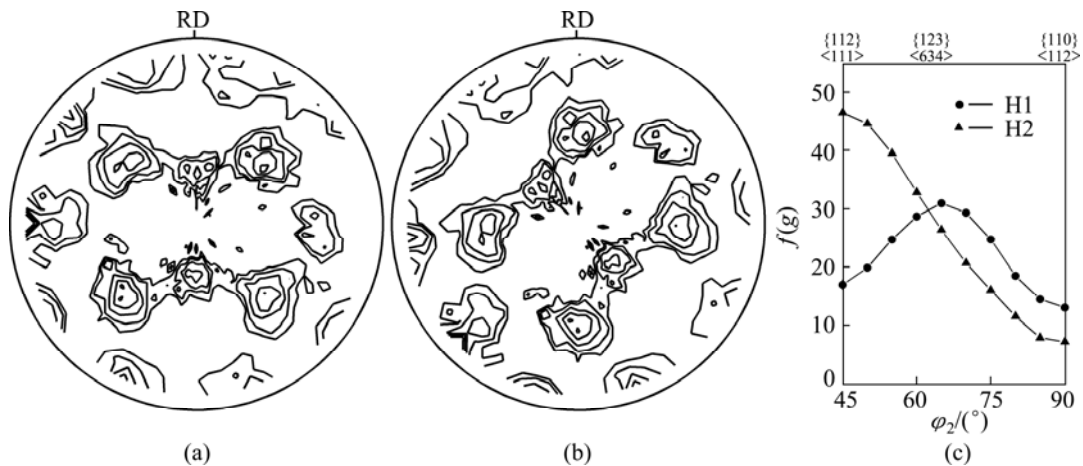


Fig. 1 Initial texture of samples H1 (a) and H2 (b) ($\{111\}$ pole figures, density levels 1, 2, 4, 8, 14) and β -fiber analysis of 95% rolling texture of samples H1 and H2 (c)

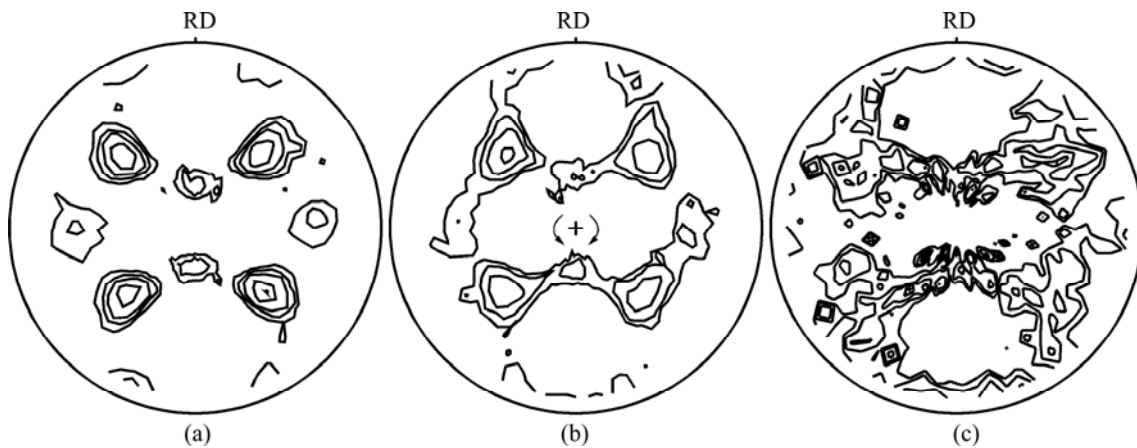


Fig. 2 Recrystallization texture of high purity aluminum sheets samples H1 (a), H2-1 (b) and H2-2 (c) ($\{111\}$ pole figures, density levels 1, 2, 4, 8, 14)

cube grains during annealing. However, according to the misorientation relationship, the strong $\{112\}\langle 111 \rangle$ rolling texture in sample H2 (Fig. 1(c)) should lead to strong $\{100\}\langle 013 \rangle$, i.e. about $\{18^\circ, 0^\circ, 0^\circ\}$ texture instead of cube texture, which was not obvious case (Fig. 2(b)). Nevertheless, the density distribution of cube texture in Fig. 2(b) does spread more in direction of ND rotation towards $\{18^\circ, 0^\circ, 0^\circ\}$ than that in Fig. 2(a) as indicated by the arrows in the center area of Fig. 2(b). Therefore, the OG effect could not be eliminated entirely while the ON effect dominated.

3.2 Influence of driving force on texture formation

The cold rolling sample H2 was also annealed at 300°C without recovery pretreatment while recrystallization process was conducted under very high stored energy and driving force. The corresponding annealed sample is indicated as H2-2 (Table 1). Higher driving force induced much more rapid recrystallization process as shown in Fig. 3. The recrystallization was not

completed yet in sample H2-1 at 300°C for 1000 s after the recovery pretreatment (Fig. 4(a)), but was almost finished in sample H2-2 at 300°C for only 2 s without pretreatment (Fig. 4(b)). 10000 s was required to complete the recrystallization process under low driving force at 300°C (Fig. 3, sample H2-1), while time less than 10 s was enough for the recrystallization under high driving forces (Fig. 3, sample H2-2).

The recrystallization texture induced by high driving force in sample H2-2 indicated a tendency to become weaker and randomized (Fig. 2(c)), which is quite different from that induced by low driving force in sample H2-1 (Fig. 2(b)).

The stored energy consists mainly of dislocation density increased by cold deformation. It is not yet possible to determine the dislocation density in deformed aluminum accurately. However, a range of the density was estimated as 10^{14} – 10^{18} m^3 [17], depending on how much the aluminum matrix has been deformed. A reduced range of 10^{14} – 10^{16} m^3 should be more rational

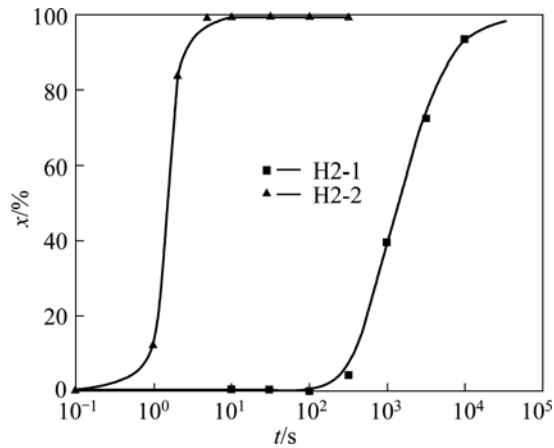


Fig. 3 Volume fraction (x) of recrystallized grains during 300 °C annealing of high purity aluminum (H2-1, recovered at 240 °C for 600 s in advance; H2-2, without recovery pretreatment)

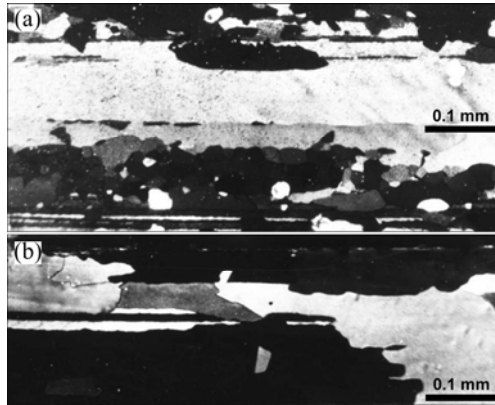


Fig. 4 Grain structure during recrystallization annealing of high purity aluminum: (a) H2-1, (240 °C, 600 s)+(300 °C, 1000 s); (b) H2-2, 300 °C, 2 s

just at the beginning of recrystallization since aluminum indicates high stacking fault energy and strong tendency of self recovery after cold deformation during temperature rising stage of recrystallization annealing. It is obvious that the recovery pretreatment at 240 °C for 600 s will reduce the stored energy further.

The relationship between radius, R , of potential nuclei in sphere and changes of Gibbs energy, ΔG , could be expressed according to conventional nucleation theory as

$$\Delta G = -\frac{4}{3}\pi R^3 \Delta G_s + 4\pi R^2 \gamma \quad (1)$$

where γ and ΔG_s are boundary energy and stored energy, respectively. If we think, in a simplified way, that the stored energy ΔG_s would consist roughly of dislocation energy Δp as driving force, which could be calculated by $\Delta p = \rho G b^2 / 2$ [15], then equation (1) could be written as

$$\Delta G = -\frac{2}{3}\rho \pi R^3 G b^2 + 4\pi R^2 \gamma \quad (2)$$

where b , G and ρ are length of Burgers vector, shear modulus and dislocation density in deformed matrix, respectively. The critical size R_c of recrystallization nuclei can be therefore deduced, which depends on dislocation density ρ . The relationship between ΔG and R at different ρ values is calculated according to Eq. (2) and shown in Fig. 5, in which $\gamma = 1 \text{ J/m}^2$ is valid [17]. The dotted vertical lines indicate the corresponding critical size R_c of nuclei at different dislocation densities.

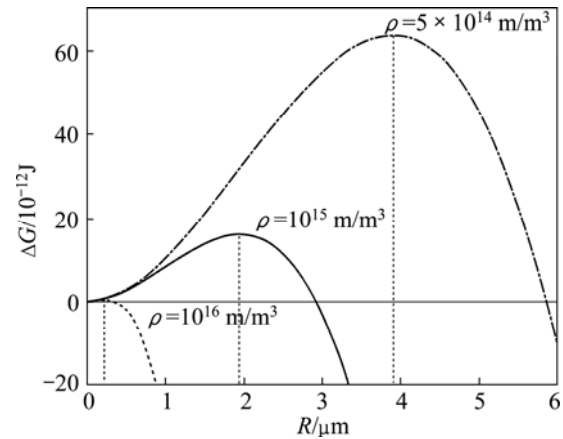


Fig. 5 Relationship between Gibbs energy ΔG and size R of potential nuclei at different dislocation densities (ρ)

The matrix of 95% rolled aluminum has been fairly recovered if intrinsic dislocation density was reduced into the range of 5×10^{14} – 10^{15} m/m^3 , while the diameters of nuclei in critical size cover several micrometers (Fig. 5). In this case an ordinary primary recrystallization could be conducted including nucleation and grain growth processes which resulted in formation of normal recrystallization texture (Figs. 2(a) and (b)). However, the deformed matrix should be less recovered if the intrinsic dislocation density maintains the level of 10^{16} m/m^3 , while the diameter of nuclei in critical size became less than 1 μm (Fig. 5). It has been observed in heavy deformed aluminum matrix [18,19] that thickness of most lamellar structure, cell blocks or sub-grains appears in the similar size range. Therefore, some cell blocks could grow as nuclei directly into the deformed matrix with rather high dislocation density (e.g. $\geq 10^{16} \text{ m/m}^3$) during annealing if they have high-angle boundaries to the matrix [18,19], while an obvious nucleation period would become no more necessary. The orientations of the cell blocks with growth advantages will determine the recrystallization texture. Figure 3(c) shows that their orientation distribution in sample H2-2 tends to appear randomly in the deformed matrix. Neither ON nor OG was detected in sample H2-2.

3.3 Influence of dragging forces on velocity of boundary migration and texture formation

There should be no obvious difference concerning intrinsic stored energy as both of the high purity and commercial purity aluminum samples, namely, samples H2 and C1, were 95% cold rolling. Figure 6 indicates that the rolling textures are characterized by strong copper texture $\{112\}\langle 111\rangle$ in both samples without serious difference. It was observed in similar commercial aluminum annealed at 500 °C for 2 h [20], that many secondary phase particles in size of 100–700 nm were distributed in the matrix with areal density of about 2000 mm^{-2} , which could drag the migration of grain boundaries during annealing. The effect is known as Zener drag p_Z [21]. On the other hand, the higher content of impurity atoms in solid solution would drag the boundary migration as well, which is known as solute drag p_s [2,21]. Therefore, higher annealing temperature is commonly applied to recrystallization of commercial purity aluminum (Fig. 7) [20].

Figure 8 indicates that an about 18° rotated cube texture $\{100\}\langle 013\rangle$ in sample C1 formed (Fig. 8(b)) [16]

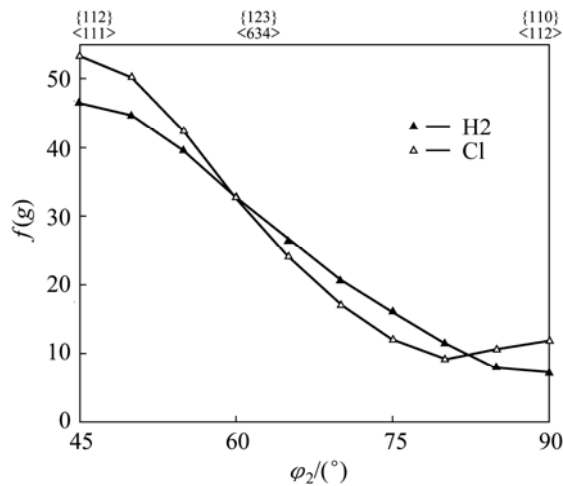


Fig. 6 β -fibers of 95% rolling texture (samples H2 and C1)

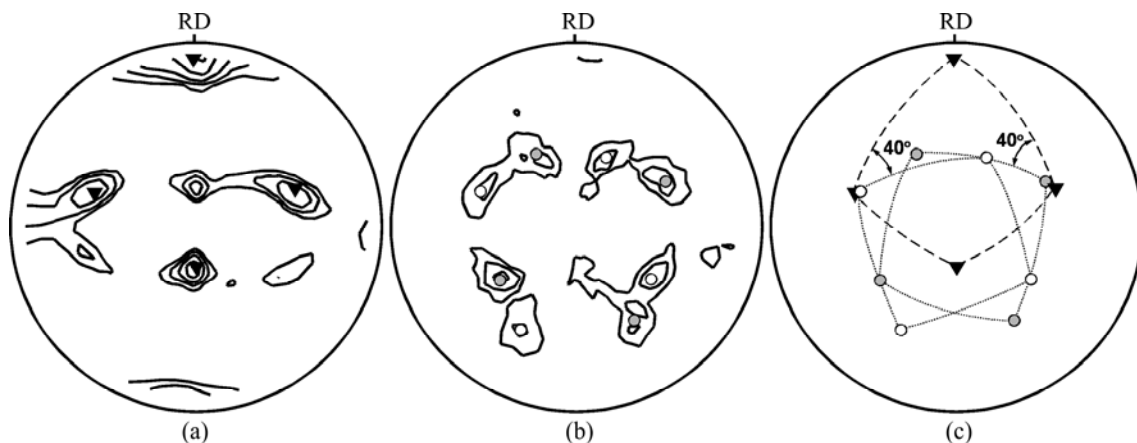


Fig. 8 Rolling (a) and recrystallization (b) texture of commercial purity aluminum sheet C1 and their orientation relationship (c) ($\{111\}$ pole figures; \blacktriangledown : $\{112\}\langle 111\rangle$; $\circ\bullet$: $\{100\}\langle 013\rangle$; density levels: 1, 2, 4, 8, 14)

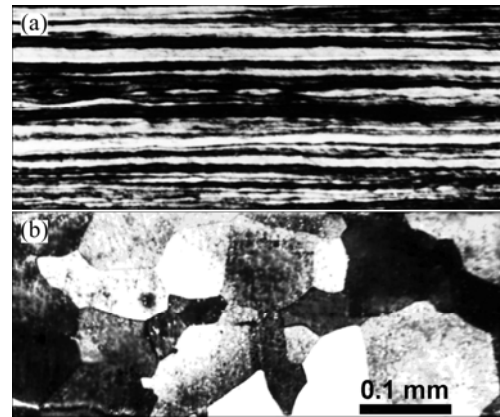


Fig. 7 Rolling and recrystallization structure of commercial purity aluminum sample C1: (a) 95% cold rolled; (b) 500 °C, 900 s, annealed

in the deformed matrix with strong copper texture $\{112\}\langle 111\rangle$ (Fig. 8(a)). The orientation relationship between $\{100\}\langle 013\rangle$ and $\{112\}\langle 111\rangle$ is just about 40° (Fig. 8(c)).

There is a simple equation to describe the Zener drag p_Z as [21]

$$p_Z = \frac{3f\gamma}{d} \quad (3)$$

where f , γ and d are volume fraction of secondary phase particle, boundary energy and average diameter of the particles, respectively. The possible volume fraction of secondary phase particles, mainly Al_3Fe particles if they fully precipitated, can be estimated as $f=0.0006$ according to the composition of sample C1 and the corresponding phase diagrams, while the level of Zener drag depends also on the average particle size d . The possible range of Zener drag p_Z and recrystallization driving force Δp can be calculated according to Eq. (3) ($\gamma=1 \text{ J/m}^2$) and $\Delta p=\rho Gb^2/2$, respectively (Fig. 9). It could be imaged that the effective driving force $\Delta p-p_Z$ and migration velocity of grain boundaries will be seriously

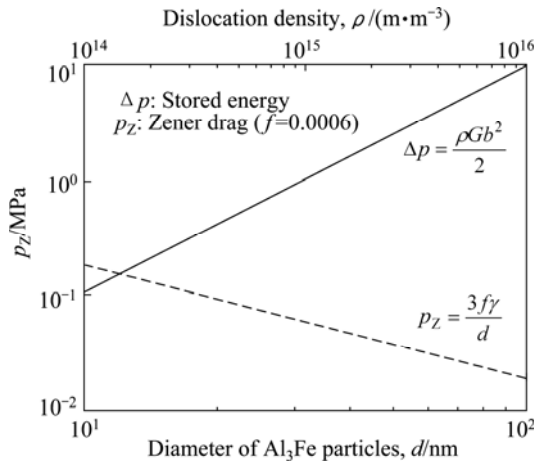


Fig. 9 Calculated Zener drag p_z for sample C1 in comparison with driving force Δp

reduced for matrix containing nano-scale particles, and the reduction should be higher than that in strong recovered sample H2-1. It seems that the mechanism of OG prevailed during annealing of sample C1. There should be certain relationship between reduced velocity of grain boundary migration and increased OG effect in consideration of similar rolling texture in samples H2 and C1 (Fig. 6).

3.4 Influence of driving force on velocity of boundary migration

An atom flux of self diffusion in aluminum crystals is proportional to $Zqv \cdot \exp[-\Delta G_D/(kT)]$, in which Z is coordination number, q is atom jumping fraction in given direction, v ($\sim 10^{13}/s$) is Debye frequency, ΔG_D is activation energy, k is Boltzmann constant and T is temperature (Fig. 10(a)). If atoms jump across a grain boundary, the corresponding activation energy ΔG_m should become generally higher than ΔG_D (Fig. 10(b)), while the increment $\Delta G_b(\theta) = \Delta G_m - \Delta G_D$ depends on misorientation angle θ of the boundary. It should be considered sometimes, that the atoms are somehow pre-activated before they jump across the boundary, since their energy state could rise in certain extent if they contact the disordered boundary directly, in which the energy increment could be expressed by ΔG_p (Fig. 10(b)).

A boundary will move in the direction with higher energy state if there is energy difference of ΔG_s between two sides of the boundary, namely, one side is annealed grain and other side is deformed grain (Fig. 10(c)). The velocity v of boundary migration could be described according to results of Burke and Turnbull [22] as

$$v = Zqv_b \left[\exp\left(-\frac{\Delta G_D + \Delta G_b(\theta) - \Delta G_s}{kT}\right) - \exp\left(-\frac{\Delta G_D + \Delta G_b(\theta)}{kT}\right) \right] \quad (4)$$

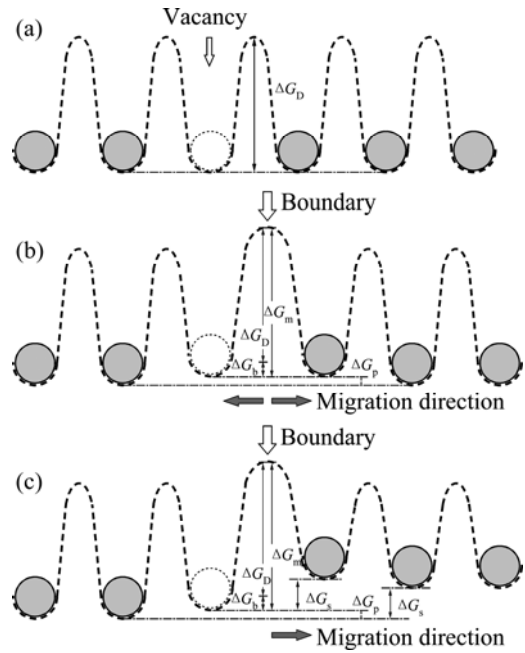


Fig. 10 Schematic illustration of atom jumps for self diffusion (a) or across boundaries (b), as well as boundary migration driven by stored energy ΔG_s (c)

where b is the length of Burgers vector.

It could be accepted that stored energy ΔG_s is replaced approximately by effective driving force $\Delta p - p_s - p_z$ for a simplified discussion, while the change of entropy during boundary migration is neglected. Then Eq. (4) could be deduced based on the first order approximation (since $\Delta p - p_s - p_z \ll kT$) as

$$v = Zqv_b \frac{\Delta p - p_s - p_z}{kT} \exp\left(-\frac{\Delta G_D}{kT}\right) \exp\left(\frac{\Delta G_b(\theta)}{kT}\right) \quad (5)$$

or

$$\begin{cases} v = v_0 \frac{\Delta p - p_s - p_z}{kT} \exp\left(-\frac{\Delta G_b(\theta)}{kT}\right) \\ v_0 = Zqv_b \exp\left(-\frac{\Delta G_D}{kT}\right) \end{cases} \quad (6)$$

while the influence of solute drag p_s and Zener drag p_z have been included as well.

3.5 Relationship between net driving force and texture formation

An ordinary discontinuous recrystallization process is completed by means of migration of high-angle boundaries. The boundary misorientation angle $\theta \approx 40^\circ$ should be much more mobile than that with any other high misorientation angle $\theta = \theta_r$, according to the mechanism of OG. A large amount of experimental observations indicated that the velocity ratio r between $v(\theta \approx 40^\circ)$ and $v(\theta = \theta_r)$ could reach one order of magnitude [1–4], namely, the maximal ratio could be as high as

about 10, which is independent on effective driving force $\Delta p - p_s - p_z$ according to Eq. (6). The ratio r could be further deduced in comparison with Eq. (6) as

$$r = \frac{v(\theta \approx 40^\circ)}{v(\theta = \theta_r)} = \exp\left(\frac{\Delta G(\theta_r) - \Delta G(40^\circ)}{kT}\right) \quad (7)$$

which indicates that OG effect would be reduced if annealing temperature becomes too high.

The recrystallization process was completed within a few seconds (Fig. 3) in high purity sample H2-2 with very high stored energy, while no obvious nucleation period was necessary. The increased orientation variety of nuclei restricted the ON effect and randomized the recrystallization texture (Fig. 2(c)). On the other hand, the recrystallization time was so limited and the grains grew so fast that those recrystallization grains, which would have obvious advantages to grow, did not have enough opportunity to expand their rapid growth ability when the primary recrystallization process had been completed already. Both ON and OG were not very efficient in this case, and a rather random ODF was also obtained (Fig. 11).

The ON became very efficient under obviously reduced stored energy when an emphasized recovery pretreatment had been conducted before the recrystallization annealing of high purity samples H1 and H2-1, after which strong cube texture formed (Fig. 2(a) and (b)). Though the misorientation between cube and S texture was just about $40^\circ \langle 111 \rangle$, the formation of cube texture was not induced mainly by OG in the deformed matrix with strong S texture in sample H1 (Fig. 1(c)), since the strong rolling copper texture did not induce 18° rotated cube texture distinctly, as predicted by OG, under the same annealing treatment. The recrystallization time and the incubation period might be still not long enough for the potential grains to expand their growth advantages. However, OG might help to strengthen the cube texture in sample H1 and induce a weak and 18° rotated cube texture in sample H2-1 (Fig. 11). Therefore, OG could not be eliminated entirely in high purity and emphatically recovered samples.

The solute drag and Zener drag in sample C1 with commercial purity reduced the net driving force, increased the recovery stage and delayed the

recrystallization process obviously, so that the recrystallization process was conducted rather slowly. Therefore, the recrystallization grains with the rotated cube orientations, which would have obvious advantages to grow into deformed matrix with copper orientations according to OG (Fig. 8(a)), did have enough time to expand their rapid growth ability before recrystallized grains had contacted each other. The formation of recrystallization texture in this case is not sensitive to whether the appreciate nuclei for OG appear earlier or later. The strong and 18° rotated cube texture formed (Fig. 8(b)), is located in the same position as that appeared slightly in sample H2-1 (Fig. 11), and there was no similar density distribution in sample H1. It could be concluded that OG prevailed during the recrystallization of sample C1.

3.6 Formation of recrystallization texture under strong Zener drag

Titanium and boron will induce formation of Al_3Ti and TiB_2 particles in aluminum alloys and could act as heterogeneous nucleation sites during solidification of aluminum melt [23,24]. Therefore, they are efficient elements reducing the grain size in aluminum (e.g. samples F1 and F2 in Table 1). Figure 12(a) gives the microstructure of sample F1 before cold rolling. It is obvious that the Al_3Ti and TiB_2 particles should distribute mainly along the grain boundaries. Many new grain boundaries were introduced inside the grains in Fig. 12(a) while they elongated along the RD during rolling. The new boundaries did not contain so many Al_3Ti and TiB_2 particles.

Figures 12(b) and (c) indicate the grain structure of sample F1 95% cold rolled and annealed at 300°C for 2 s and 10 s, respectively. The recrystallization grains could not grow in the deformed matrix freely, which is different from that shown in sample C1 (Fig. 7(b)). It seems that the grain growth in the initial stage of recrystallization (Fig. 12(b)) was limited in the grain before cold rolling (Fig. 12(a)). Therefore, the Al_3Ti and TiB_2 particles indicated much stronger Zener dragging effect against the boundary migration than Al_3Fe particles in sample C1. The grain growth could later

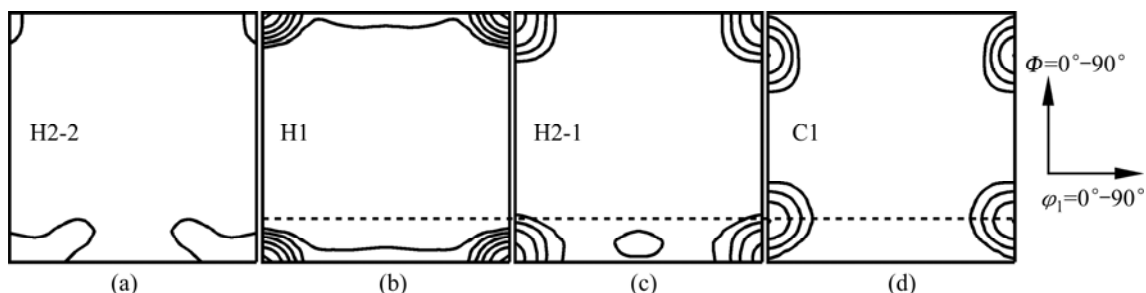


Fig. 11 ODF $\phi_2=0^\circ$ sections of annealed samples H2-2, H1, H2-1 and C1 (from left to right, density levels: 6, 12, 20, 30, 42, 56)

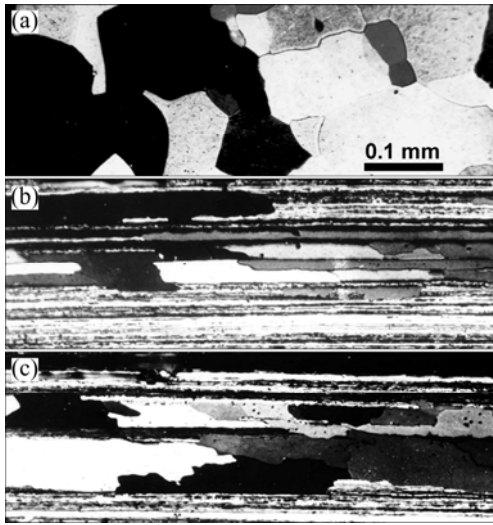


Fig. 12 Microstructures of sample F1: (a) Before cold rolling; (b) 95% cold rolling at 300 °C for 2 s, annealed; (c) 95% cold rolling at 300 °C for 10 s, annealed

pervade across the boundaries existing before cold rolling (Fig. 12(c)), while the grain orientation had been determined already. The characterized grain growth behaviors will influence the formation of recrystallization texture.

Figure 13 shows the texture evolutions during the rolling and annealing of samples F1 and F2. There were initial textures before cold rolling (Table 1). The initial $\{110\}\langle 001 \rangle$ texture led to strong brass texture $\{110\}\langle 112 \rangle$ after 95% cold rolling in sample F1 while the instable $\{110\}\langle 221 \rangle$ texture disappeared (Fig. 13). The initial

$\{110\}\langle 114 \rangle$ texture in sample F2 resulted in strong rolling texture $\{110\}\langle 112 \rangle$ while the instable $\{110\}\langle 110 \rangle$ texture vanished (Fig. 13). A strong recovery pretreatment had been conducted at 240 °C for 10 min, while the effective driving force was drastically reduced. A $\{110\}\langle 001 \rangle$ or $\{110\}\langle 114 \rangle$ recrystallization texture formed in samples F1 and F2 beside cube texture after annealing at 300 °C. The OG behaviors were not observed, which is quite different from that in sample C1.

It is clear, however, that the ON mechanism played an important role in determining the recrystallization textures. The weak cube texture before rolling became strong after annealing (Fig. 13), and the formation mechanism should be similar to that in sample H1 based on ON. Figure 14 gives the α -fiber analyses of samples F1 and F2 before rolling during annealing. Obvious $\{110\}\langle 001 \rangle$ (sample F1) and $\{110\}\langle 114 \rangle$ (sample F2) recrystallization textures formed around the positions before rolling, which indicates a strong ON effect. Some $\{110\}\langle 001 \rangle$ textures formed also in sample F2 after annealing (Fig. 14(b)), which could be explained by the mechanism of ON as well. The nuclei in the initial stage of recrystallization did not obtain enough space to grow in consideration of observations in Figs. 12(b) and (c). The space was so limited (Fig. 12(b)) that those recrystallization grains, which would have obvious advantages to grow, did not have enough opportunity to expand their rapid growth ability. Therefore the possibility for OG was drastically reduced. It could be understood that the ON effect exists all the time if the

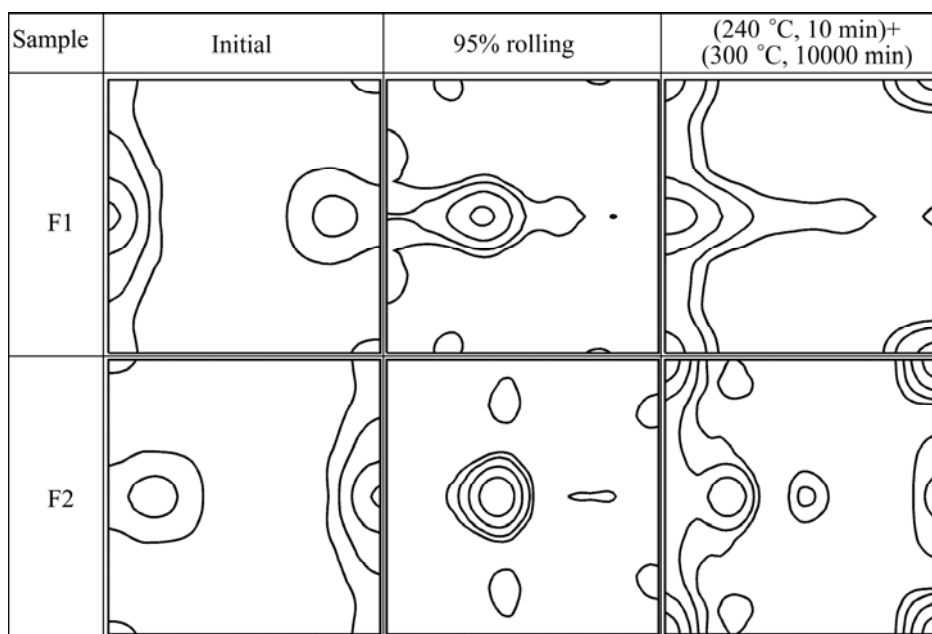


Fig. 13 ODF $\varphi_2=0^\circ$ sections of samples F1 and F2 at initial stage, after 95% rolling and after annealing at (240 °C, 10 min)+(300 °C, 10000 s) (density levels: 2, 4, 8, 14)

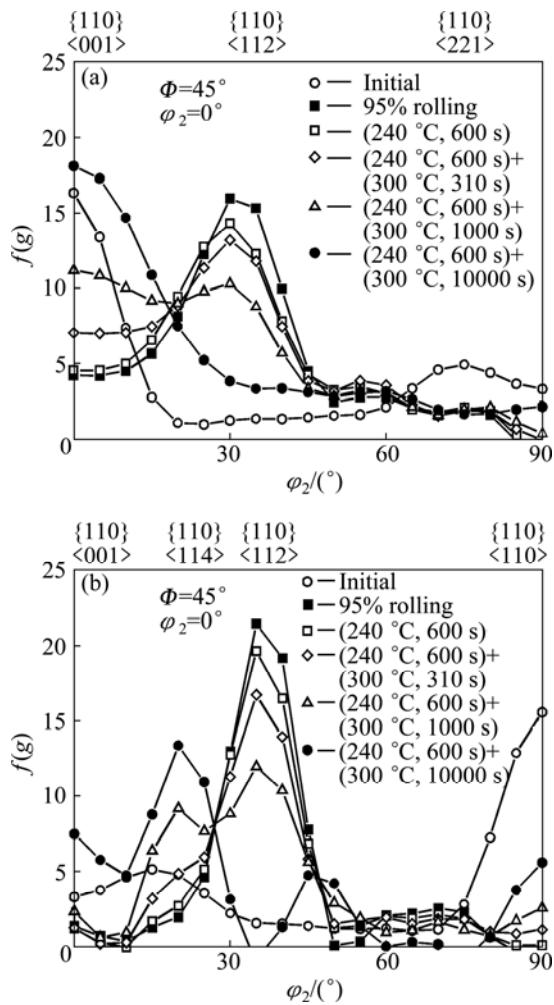


Fig. 14 α -fiber analysis of samples F1(a) and F2(b) before cold rolling during annealing

effective driving force is not too high and could be observed clearly if the OG effect does not obtain the opportunity to enshroud ON.

4 Conclusions

1) The basic behavior in initial stage of primary recrystallization in aluminum is that some cell blocks and sub-grains are transformed into or even directly become nuclei, of which the orientation variety and prominence of ON depend on the level of driving force. Too higher effective driving force $\Delta p - p_s - p_z$ leads to increase of orientation variety and reduction of prominent ON. Otherwise, ON should be general behaviors at the initial stage of recrystallization. OG may happen during annealing; however, it needs time and space to expand its advantages on growth selection and determining recrystallization texture. OG effect will be reduced obviously if the grain growth period for primary recrystallization becomes very short due to too high driving force, or if grain growth space in deformed

matrix becomes very limited because of high density of secondary phase particles at the boundaries before deformation and corresponding strong dragging effects. OG effect would be also reduced if the annealing temperature becomes too high.

2) It could be imaged that the control of initial texture, recovery process and effective driving force before recrystallization of deformed aluminum could be applied to changing the recrystallization texture. Therefore, quantitative investigations concerning the relations among initial textures, levels of recovery, matrix purity, dragging effects, levels of effective driving force, mechanisms of texture formation and following recrystallization textures need to be conducted.

References

- [1] IBE G, DIETZ W, FRAHER A C, LÜCKE K. Vorzugsorientierung bei der rekristallisation gedehnter einkristalle aus reinst-aluminium [J]. Zeitschrift für Metallkunde, 1970, 61(7): 498–507. (in German)
- [2] MOLODOV D A, CZUBAYKO U, GOTTSTEIN G, SHVINDLERMAN L S. On the effect of purity and orientation on grain boundary motion [J]. Acta Materialia, 1998, 46(2): 553–564.
- [3] TAHERI M L, ROLLETT A D, WEILAND H. In-situ quantification of solute effects on grain boundary mobility and character in aluminum alloys during recrystallization [J]. Mater Sci Forum, 2004, 467–470: 997–1002.
- [4] TAHERI M L, MOLODOV D, GOTTSTEIN G, ROLLETT A D. Grain boundary mobility under a stored-energy driving force: A comparison to curvature-driven boundary migration [J]. Zeitschrift für Metallkunde, 2005, 96(10): 1166–1170.
- [5] KRONBERG M L, WILSON F H. Secondary recrystallization in copper [J]. Trans Met Soc AIME, 1949, 185: 501–514.
- [6] MAO W M. Model for rapidly moving boundaries [J]. Science in China A, 1992, 35: 336–343.
- [7] MAO W M. Atomistic model of rapid moving grain boundaries in FCC metals [J]. Mater Sci Forum, 2002, 408–412: 269–274.
- [8] DILLAMORE I L, KATOH H. The mechanisms of recrystallization in cubic metals with particular reference to their orientation dependence [J]. Metal Science, 1974, 8: 73–83.
- [9] MAO W M. Formation of recrystallization cube texture in high purity FCC metal sheets [J]. Journal of Materials Engineering & Performance, 1999, 8: 556–560.
- [10] RIDHA A A, HUTCHINSON B. Recrystallization mechanisms and the origin of cube texture in copper [J]. Acta Met, 1982, 30: 1929–1939.
- [11] ALVI M H, CHEONG S W, SUNI J P, WEILAND H, ROLLETT A D. Cube texture in hot-rolled aluminum alloy 1050 (AA1050)—Nucleation and growth behavior [J]. Acta Materialia, 2008, 56: 3098–3108.
- [12] MAO W M. Modeling of rolling texture in aluminum [J]. Mater Sci Eng A, 1998, 257: 171–177.
- [13] MAO W M. Rolling texture development in aluminum [J]. Chin J Mat Sci Technol, 1991, 7: 101–112.
- [14] HUTCHINSON B. The cube texture revisited [J]. Mater Sci Forum, 2012, 702–703: 3–10.
- [15] MAO W M. Recrystallization and grain growth [M]//Handbook of Aluminum, Physical Metallurgy and Processes, Vol.1. New York: Marcel Dekker Inc, 2003: 211–258.
- [16] MAO W M, YANG P. Effects of driving force and boundary migration velocity on formation of recrystallization texture in cold

- rolled pure aluminum sheets [J]. Mater Sci Forum, 2013, 753: 257–262.
- [17] MONDOLFO L F. Aluminum alloys: Structure and properties [M]. London: Butterworths, 1976: 11–20.
- [18] LIU Q, HUANG X, LLOYD D J, HANSEN N. Microstructure and strength of commercial purity aluminium (AA 1200) cold-rolled to large strains [J]. Acta Materialia, 2002, 50: 3789–3802.
- [19] HUANG X, TSUJI N, HANSEN N, MINAMINO Y. Microstructural evolution during accumulative roll-bonding of commercial purity aluminum [J]. Mater Sci Eng A, 2003, 340: 265–271.
- [20] AMBAT R, DAVENPORT A J, SCAMANS G M, AFSETH A. Effect of iron-containing intermetallic particles on the corrosion behaviour of aluminium [J]. Corrosion Science, 2006, 48: 3455–3471.
- [21] HUMPHREYS F J, HATHERLY M. Recrystallization and related annealing phenomena [M]. 2nd ed. Amsterdam: Elsevier, 2004, 112–119.
- [22] BURKE J E, TURNBULL D. Recrystallization and grain growth [M]//Progress in Metal Physics 3. London: Pergamon Press, 1952: 220–292.
- [23] EASTON M A, STJOHN D H. A model of grain refinement incorporating alloy constitution and potency of heterogeneous nucleant particles [J]. Acta Materialia, 2001, 49: 1867–1878.
- [24] VENKATESWARLU K, CHAKRABORTY M, MURTY B S. Influence of thermo-mechanical processing of Al–5Ti–1B master alloy on its grain refining efficiency [J]. Mater Sci Eng A, 2004, 364: 75–83.

基于选择形核和选择生长理论的 铝板再结晶组织形成机制

毛卫民, 杨平

北京科技大学 新金属材料国家重点实验室 材料学系, 北京 100083

摘要: 研究不同纯度和初始结构铝板经 95%冷轧后的再结晶组织。分析回复程度和杂质钉扎效应对退火过程中定向形核和选择生长行为的影响。在初次再结晶的开始阶段, 若变形基体内有效驱动力不是特别高, 在不缩短形核周期的情况下, 通常会有定向形核行为出现。若温度不是特别高以致与基体保持约 $40^\circ\langle 111 \rangle$ 取向差关系的晶粒有充分的时间优先长大, 则也会出现选择性生长, 此时也需使有效驱动力有所降低。借助控制初始结构或用回复程度和钉扎效应调整有效驱动力可以改变再结晶组织。

关键词: 铝; 再结晶; 组织; 回复; 储存能; 晶界迁移

(Edited by Xiang-qun LI)